RSC Advances

PAPER

View Article Online
View Journal | View Issue

Cite this: *RSC Adv.*, 2021, **11**, 11943

Flexible poly(vinylidene fluoride-*co*-hexafluoropropylene)-based gel polymer electrolyte for high-performance lithium-ion batteries

Pan Zhang,[a] Rui Li,[a] Jian Huang,[a] Boyu Liu,[a] Mingjiong Zhou,*[a] Bizheng Wen,*[b] Yonggao Xia[c] and Shigeto Okada[d]

Gel polymer electrolytes (GPEs) have attracted ever-increasing attention in Li-ion batteries, due to their great thermal stability and excellent electrochemical performance. Here, a flexible poly(vinylidene fluoride-*co*-hexafluoropropylene) (PVDF-HFP)-based GPE doped with an appropriate proportion of the PEO and SiO_2 is developed through a universal immersion precipitation method. This porous PVDF-HFP-PEO-SiO_2 GPE with high ionic conductivity and lithium-ion transference number (t_{Li^+}) can enhance the electrochemical performance of $LiFePO_4$ cells, leading to superior rate capability and excellent cycling stability. Moreover, the PVDF-HFP-PEO-SiO_2 GPE effectively inhibits the lithium dendrite growth, thereby improving the safety of Li-ion batteries. In view of the simplicity in using the gel polymer electrolyte, it is believed that this novel GPE can be used as a potential candidate for high-performance Li-ion batteries.

Received 15th February 2021
Accepted 16th March 2021

DOI: 10.1039/d1ra01250a

rsc.li/rsc-advances

1. Introduction

With the rapid development of portable electronic devices and electric vehicles, lithium-ion batteries (LIBs) have been widely used due to their high specific capacity, low self-discharge, high battery voltage, long cycling life and environmental friendliness.[1–3] However, the organic solvent in the traditional liquid electrolyte is flammable, thus it can cause spontaneous combustion and even explosion accidents, which severely hinders the development of LIBs.[4] Therefore, to improve the safety of LIBs, solid electrolytes have received extensive attention from researchers due to their non-flammability and wide working temperature range, and lithium metal can be chosen as the anode.[5,6] However, the low ionic conductivity and poor interfacial contact between electrodes and solid-state electrolytes restrict the practical application.[7,8]

Gel polymer electrolytes (GPEs) have an intermediate state between solid and liquid, formed by immersing the polymer membrane in the liquid electrolyte, which can simultaneously provide the high ionic conductivity of liquid electrolytes at room temperature and the excellent safety of solid-state electrolytes.[9,10] GPEs are mainly composed of three parts: polymer matrix, lithium salt and low-molecular organic solvent (plasticizer). The polymer matrix is the core of the GPEs structure, and plays a role in adsorbing plasticizers.[11,12] The ideal GPEs must exhibit high room temperature ion conductivity, lithium-ion transference number, electrochemical stability window and mechanical strength, *etc.*[13–16] Recently, the polymers have been widely studied, such as poly(ethylene oxide) (PEO),[17] poly(methyl methacrylate) (PMMA),[18–20] poly(vinyl chloride) (PVC),[21] poly(acrylonitrile) (PAN),[22–24] poly(vinylidene fluoride) (PVDF),[25] and poly(vinylidene fluoride-*co*-hexafluorpropylene) (PVDF-HFP).[1,26,27] Among them, the high electron-absorption C–F bonds of PVDF-HFP polymer has attracted great interest from scientific researchers, due to its excellent thermal endurance, superior dielectric constant, good mechanical performance, and high electrochemical stability.[27] The copolymer PVDF-HFP obtained by introducing amorphous HFP into PVDF can disrupt the symmetric and regular chain structure of pure PVDF to reduce its crystallinity, thereby enhancing the adsorption of the polymer membrane to the liquid electrolyte and improving the conductivity of GPEs.

The addition of ceramic nanoparticles such as SiO_2,[28,29] TiO_2,[30] Al_2O_3,[31] and ZrO_2 (ref. 32) can further improve the performance of GPEs. The inorganic filler in the polymer matrix can increase the proportion of the amorphous region of the polymer chain, reduce the crystallinity of the polymer membrane, as well as increase the Li^+ conductivity. Because of the high heat resistance of inorganic fillers, they are beneficial

[a]*School of Materials Science and Chemical Engineering, Ningbo University, Fenghua Road 818, Ningbo 315211, Zhejiang Province, People's Republic of China. E-mail: zhoumingjiong@nbu.edu.cn*

[b]*Ningbo Procutivity Promotion Center, Yangfan Road 999, Hi-tech Zone, Ningbo 315100, Zhejiang Province, People's Republic of China. E-mail: 121001627@qq.com*

[c]*Ningbo Institute of Industrial Technology, Chinese Academy of Science, Ningbo 315201, Zhejiang Province, People's Republic of China*

[d]*Institute for Materials Chemistry and Engineering, Kyushu University, 6-1 kasuga-koen, kasuga 816-8580, Japan*

to improve the thermal stability of GPE. In addition, inorganic nanoparticles can also enhance the mechanical strength and interface stability of GPEs.

In this work, a PVDF-HFP-based porous GPE with a proper proportion of the PEO and SiO_2 was prepared by immersion precipitation method. Since the oxygen-containing functional groups of PEO segment have excess electrons, lithium ions become easy to coordinate with the ether oxygen functional groups.[17] The hydrophilicity of PEO can increase the exchange rate of solvent and non-solvent, thereby promoting the formation of finger-like pore structure.[33–35] Herein, with the addition of the PEO and SiO_2, the PVDF-HFP-PEO-SiO_2 GPE showed low crystallinity, excellent thermal stability, wide electrochemical window, high lithium-ion transference number and ionic conductivity. The 3D porous structure of PVDF-HFP-PEO-SiO_2 GPE provided higher porosity and liquid electrolyte uptake than pure PVDF-HFP GPE. Moreover, the obtained CPE exhibited a wide electrochemical window up to 4.7 V, enhanced ionic conductivity of 1.12×10^{-3} S cm^{-1}, and higher lithium-ion transference number (t_{Li^+}) of 0.48. Notably, the capacity of the $LiFePO_4$ cell with PVDF-HFP-PEO-SiO_2 GPE remained at 146.3 mA h g^{-1} even after 200 cycles at 0.1C. The lithium symmetric battery assembled with the PVDF-HFP-PEO-SiO_2 GPE also displayed ultralong cycling life. It is believed that this novel GPE has a great potential to be used for high safety lithium metal batteries in practical application.

2. Experimental

2.1 Materials

Poly(ethylene oxide) (PEO, $M_w \approx 600\,000$), bis(trifluoromethanesulfoneimide) lithium salt (LiTFSI, 99.9%), and nano SiO_2 powder was purchased from Macklin. Poly(vinylidene fluoride-*co*-hexafluorpropylene) (PVDF-HFP, $M_w \approx 455\,000$) was purchased from Sigma-Aldrich. *N*-Methyl-2-pyrrolidone (NMP) and *N*,*N*-dimethylformamide (DMF) was purchased from Sigma-Aldrich. Poly(vinylidene fluoride) (PVDF), lithium iron phosphate ($LiFePO_4$), conductive carbon black (Super P), ethylene carbonate (EC) and dimethyl carbonate (DMC) were purchased from Guangdong Canrd New Energy Technology Co., Ltd.

2.2 Preparation of the PVDF-HFP-PEO-SiO_2 gel polymer electrolyte

The composite polymer membrane with porous structure was prepared by immersion precipitation method. PVDF-HFP was dissolved in DMF with a weight percent of 10 wt% and magnetically stirred at 60 °C for 2 h to form a homogeneous and transparent solution. After that, PEO and SiO_2 (both of them were 10 wt% of PVDF-HFP) were added to the above solution and stirred at 60 °C for 2 h. The obtained viscous solutions were casted on a clean glass plate, and then put into deionized water. After the phase inversion was completed, the PVDF-HFP-PEO-SiO_2 membrane fell off the glass plate. Finally, freeze-dry the PVDF-HFP-PEO-SiO_2 membrane for 24 h to completely remove the water and residual DMF. For comparison, the pure PVDF-HFP membrane was also prepared by the same method. All the as-prepared polymer membranes were cut into 18 mm in diameter and transferred into an Ar-filled glovebox (H_2O < 0.1 ppm, O_2 < 0.1 ppm) for further testing and characterization. The prepared PVDF-HFP-PEO-SiO_2 membrane was soaked in the liquid electrolyte (1 M LiTFSI in EC/DMC, 1/1 by volume) for 2 h, and the excess liquid electrolyte on the membrane was removed by wiping with a filter paper.

2.3 Characterization of the composite separators

The surface morphology of all the samples was characterized by scanning electron microscope (SEM, Hitachi S-4800). Thermal gravimetric analysis (TGA) curves were performed under nitrogen (N_2) atmosphere with a heating rate of 10 °C min^{-1} using a Netzsch STA 2500. The crystallinity was measured by X-ray diffraction (XRD, Bruker D8 Advance) using Cu Ka radiation. The diffraction angle (2θ) was between 5° and 80° with a scan rate of 5° min^{-1}. The tensile mechanical performance tests were performed on an electronic universal testing mechine (UTM, 6530, Shenzhen Kay Strength Test Instrument Co., Ltd.) at room temperature with a stretching speed of 20 mm min^{-1}.

The degree of crystallinity (X_c) of the different membranes was obtained by the following eqn (1):[36]

$$\text{Crystallinity}(\%) = \frac{\text{area of cryatallinity peaks}}{\text{area of all peaks}} \times 100\% \quad (1)$$

The electrolytes uptake of the different membranes was calculated by the following eqn (2):[1]

$$\text{Electrolyte uptake}(\%) = \frac{M_2 - M_1}{M_1} \times 100\% \quad (2)$$

where M_1 and M_2 are the weights of the different membranes before and after immersion in the liquid electrolytes.

The porosity was obtained from the following method. The different membranes were first soaked in *n*-butanol for 2 h, and then wiped off the excess *n*-butanol on the membrane surface with a filter paper. The wet membranes were weighed immediately. The porosity of the membranes was obtained by the following eqn (3):[1,36]

$$\text{Porosity}(\%) = \frac{\Delta M}{\rho V_0} \times 100\% \quad (3)$$

ΔM is the mass of the membranes after and before the adsorption of *n*-butanol, ρ is the density of *n*-butanol, and V_0 is the membrane volume before the adsorption of *n*-butanol.

2.4 Measurements of electrochemical performance

The ionic conductivity was tested by an electrochemical workstation. The separators were sandwiched between two stainless steel (SS) electrodes, and measured by AC impedance spectroscopy in the frequency range from 1.0 MHz to 0.01 Hz with an AC amplitude of 10 mV. The ionic conductivity was calculated by the following eqn (4):[13,36]

$$\sigma = \frac{d}{R \times S} \quad (4)$$

where σ is the ionic conductivity, d is the thickness of the separators, R is the bulk resistance, and S is the area of the separators.

The lithium-ion transference number (t_{Li+}) of the symmetric Li|GPE|Li battery was measured by the chronoamperometry and the AC impedance spectroscopy with a voltage of 10 mV. The lithium-ion transference number (t_{Li+}) was obtained by the following eqn (5):[36]

$$t_{Li^+} = \frac{I_{ss}\ (\Delta V - I_0 R_0)}{I_0\ (\Delta V - I_{ss} R_{ss})} \quad (5)$$

where I_0 and I_{ss} are the initial and steady-state current, respectively. R_0 and R_{ss} are the initial and steady-state interfacial resistance, respectively. ΔV is the polarization potential (10 mV).

The electrochemical stability window was tested by sandwiching the separators between stainless steel (SS) and lithium metal as the working electrode and the counter electrode, respectively. The voltage range was from 0 to 6.0 V with a scan rate of 10 mV s^{-1}. The electrochemical properties were carried out using CR2032 coin-type of Li/GPE/$LiFePO_4$ on the battery test system (Wuhan Land Electronic Co. Ltd., China). The $LiFePO_4$ cathode was prepared by completely mixing $LiFePO_4$ active powder, Super P, and PVDF with a mass ratio of 80 : 10 : 10 in *N*-methyl-2-pyrrolidone (NMP) solvent. Subsequently, the slurry was coated onto an aluminum foil, and dried at 100 °C for 24 h in a vacuum oven, and then punched to 10 mm diameter disk for testing. The mass loading of the as-prepared $LiFePO_4$ cathode was about 1.25 mg cm^{-2}. Cells were assembled in a glove-box filled with argon. The galvanostatic charge–discharge tests were carried out at a constant current density in a voltage range of 2.6–4.0 V. The Li/Li symmetric cells were assembled by sandwiching the GPE between two lithium foils.

3. Results and discussion

SEM was used to illustrate the influence of PEO introduction on the structure of the polymer membrane. Fig. 1a–f shows the SEM images of the bottom surface, top surface and cross-section of the pure PVDF-HFP and PVDF-HFP-PEO-SiO_2 membrane, respectively. As shown in Fig. 1a, almost no penetrating pores were found on the bottom surface of the pure PVDF-HFP membrane, but only slight concave was observed on the bottom surface. The pure PVDF-HFP membrane showed a relatively dense top surface (Fig. 1b), and the thickness of the pure PVDF-HFP membrane was about 100 μm (Fig. 1c). It was further confirmed that the length of the finger-like pore structure was about one-third of the entire cross-section, and the remaining parts formed a sponge-like pore structure. After the addition of the PEO and SiO_2, the microstructure of the polymer membrane became more porous with improved pore interconnectivity, which can be observed from Fig. 1d and e. Meanwhile, it can be observed that the cross-section of the PVDF-HFP-PEO-SiO_2 membrane with penetrating finger-like pore structure (Fig. 1f). The PEO was a hydrophilic polymer, which could increase the exchange rate of solvent and non-solvent during the preparation process, thereby promoting the formation of finger-like pore structure.[34] Since the porous structure was beneficial for absorbing more liquid electrolyte, the ionic conductivity of the GPE can be enhanced significantly.[1,36]

To obtain thermal dimensional stability of the polymer membrane, the Celgard 2325 separator, pure PVDF-HFP and PVDF-HFP-PEO-SiO_2 were heat-treated for 1 h at 150 °C and 175 °C, respectively. Fig. 2a and b display photographs of the separators and the corresponding shrinkage ratios before and after heat treatment, respectively. The Celgard 2325 separator exhibited serious shrinkage after thermal treatment at elevated temperature. When the temperature increased from 150 °C to 175 °C, the shrinkage ratio of the Celgard 2325 separator changed from 22% to 36%. In contrast, the dimensional changes of the pure PVDF-HFP and PVDF-HFP-PEO-SiO_2 were only 4% at 150 °C. Furthermore, both the pure PVDF-HFP and PVDF-HFP-PEO-SiO_2 did not exhibit significant dimensional changes at higher temperature of 175 °C. These results suggested that the PVDF-HFP-based membranes had much better thermal stability compared to the Celgard 2325 separator, which implied that the PVDF-HFP-based membrane as a separator can improve the battery safety by reducing the risk of short circuit.

Fig. 2c shows TG curves of the Celgard 2325 separator and PVDF-HFP-based membranes. A strong mass loss occurred at about 260 °C for the Celgard 2325 separator, while the PVDF-HFP membrane started to decompose at around 415 °C, indicating the good thermal stability of polymer PVDF-HFP. However, the PVDF-HFP-PEO-SiO_2 has a relatively lower initial decomposition temperature of ~350 °C than pure PVDF-HFP with the addition of PEO and SiO_2. The lower initial decomposition temperature should be related to the addition of PEO.[4] In addition, PVDF-HFP-based membranes display a higher residual amount than Celgard 2325 separator. Hence, PVDF-HFP-PEO-SiO_2 membrane with great thermal stability can be utilized as the separator for applications in LIBs with high safety.

The crystalline structures of the Celgard 2325 separator, pure PVDF-HFP and PVDF-HFP-PEO-SiO_2 membranes were performed by XRD, as shown in Fig. 3a. Obviously, two intense characteristic peaks at 18.3° and 19.9° were observed for the pure PVDF-HFP membrane. After addition of the PEO and SiO_2, the characteristic peak of the PVDF-HFP membrane slightly decreased. In addition, the degree of crystallinity (X_c) was calculated by the eqn (1). The X_c of the Celgard 2325 separator, pure PVDF-HFP and PVDF-HFP-PEO-SiO_2 membrane were 36%, 39% and 27%, respectively. The introduction of the PEO and SiO_2 can significantly reduce the crystallinity of the PVDF-HFP-based membrane, which was agreed well with the XRD results. The decrease of crystallinity can be considered as the addition of nano-filler SiO_2 disrupted the chain structure of pure PVDF-HFP, resulting in the reduce of crystalline zone, and thus enhanced the transport of lithium ions.[17,37]

The porosity and liquid electrolyte uptake were used to further explore the porous structure of the polymer membrane. Fig. 3b shows the porosity of various membranes, together with

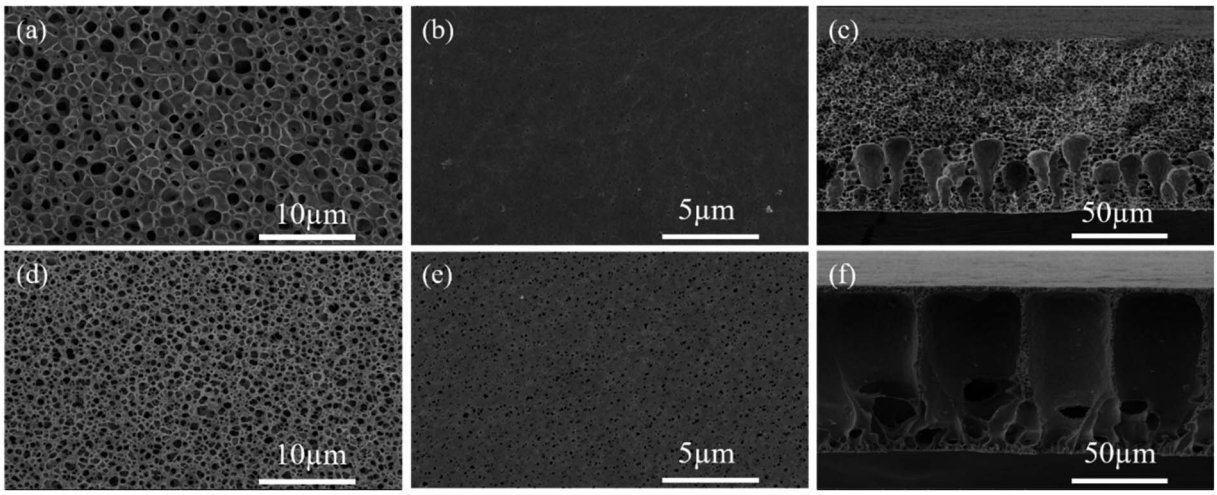

Fig. 1 SEM images of (a) bottom surface, (b) top surface and (c) cross section of PVDF-HFP membrane. SEM images of (d) bottom surface, (e) top surface and (f) cross section of PVDF-HFP-PEO-SiO_2 membrane.

the corresponding liquid electrolyte uptake. The porosity of PVDF-HFP-PEO-SiO_2 reached 74%, which was much higher than the Celgard 2325 separator (25%) and the pure PVDF-HFP (41%). The corresponding liquid electrolyte uptake of the Celgard 2325 separator, pure PVDF-HFP and PVDF-HFP-PEO-SiO_2 were 126%, 181% and 539%, respectively. Obviously, the addition of PEO and SiO_2 effectively increased the porosity of PVDF-HFP, which can absorb more liquid electrolyte and get higher lithium ion conductivity.[1] Fig. 3c shows the mechanical property of the PVDF-HFP-PEO-SiO_2 GPE. The tensile strength of the PVDF-HFP-PEO-SiO_2 GPE was 6.72 MPa with an elongation-at-break at 80%. The higher mechanical property of PVDF-HFP-PEO-SiO_2 GPE decreased the risk of short-circuit of lithium batteries, improving their safety and stability.

The electrochemical window of the Celgard 2325 separator with liquid electrolyte and PVDF-HFP-based GPEs were recorded with linear sweeping voltammetry (LSV) curves in the voltage range of 0–5.5 V at a scan rate of 10 mV s^{-1}. As shown in Fig. 4a, the anodic limiting potential of PVDF-HFP-based GPEs was higher than that of the Celgard 2325 separator absorbed liquid electrolyte (~4.5 V). Moreover, it can be observed that the PVDF-HFP-PEO-SiO_2 GPE showed the highest anodic limiting potential of 4.7 V. Hence, the addition of the PEO and SiO_2 was supposed to improve the electrochemical stability of the PVDF-HFP-PEO-SiO_2 GPE for LIBs.[17,37]

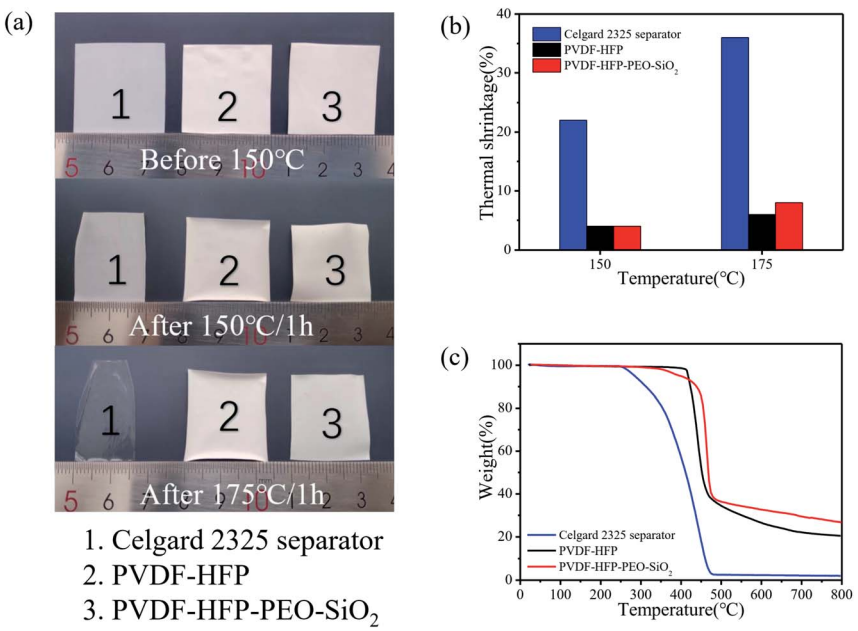

Fig. 2 (a) Photographs of the Celgard 2325 separator and PVDF-HFP-based membranes before and after being exposed to 150 °C and 175 °C for 1 h. (b) Thermal shrinkage of membranes after heat-treatment. (c) TG curves for various membranes.

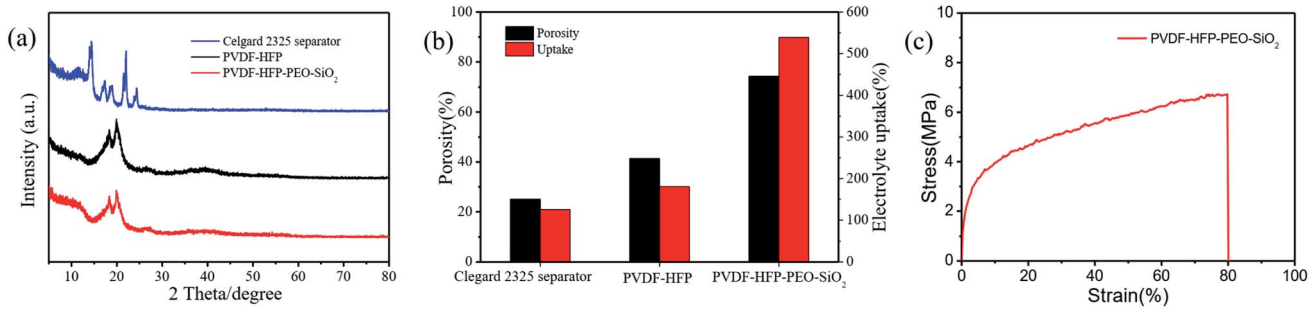

Fig. 3 (a) XRD patterns, (b) porosity and electrolyte uptake of the Celgard 2325 separator, pure PVDF-HFP and PVDF-HFP-PEO-SiO_2, (c) stress–strain curve of the PVDF-HFP-PEO-SiO_2 GPE.

The ionic conductivity was measured by an AC impedance analyzer technique, and the values were calculated by the eqn (4). As shown in Fig. 4b, the ionic conductivity of the PVDF-HFP-based GPEs was much higher than that of the Celgard 2325 separator absorbed liquid electrolyte. The ionic conductivity of the Celgard 2325 separator that absorbed liquid electrolyte, pure PVDF-HFP and PVDF-HFP-PEO-SiO_2 GPEs can be calculated to be 4.33×10^{-5} S cm^{-1}, 2.46×10^{-4} S cm^{-1}, and 1.12×10^{-3} S cm^{-1}, respectively. Moreover, the ionic conductivity of PVDF-HFP-PEO-SiO_2 GPE was slightly lower than that of the liquid electrolyte (7.86×10^{-3} S cm^{-1}). The improvement of ion conductivity was attributed to the following reasons. First, fluorine atom of PVDF-HFP has strong electronegativity, which can facilitate the lithium ions to transfer easily in the amorphous region. Second, the oxygen-containing functional groups of PEO segment have excess electrons, while the electron orbitals of lithium ions contain empty orbitals, thus lithium ion becomes easy to coordinate with the ether oxygen functional groups.[17,19] Third, the PVDF-HFP-PEO-SiO_2 GPE with high porosity and good pore interconnectivity increased the electrolyte uptake ratio.[1] The high ionic conductivity of the PVDF-HFP-PEO-SiO_2 GPE should be beneficial for the effective enhancement of battery performance.

The lithium-ion transference number (t_{Li^+}) is an important parameter of the GPEs, which influences the electrochemical properties of LIBs. The value of t_{Li^+} was calculated by the eqn (5), where the initial and steady-state current were obtained by the polarization curve, and the initial and steady-state interface impedances were obtained by AC impedance, as shown in Fig. 5. The PVDF-HFP-PEO-SiO_2 GPE reached a high t_{Li^+} of 0.49, which was higher than those of the pure PVDF-HFP GPE ($t_{Li^+} = 0.39$) and the Celgard 2325 separator absorbed liquid electrolyte ($t_{Li^+} = 0.27$). The higher t_{Li^+} of the PVDF-HFP-PEO-SiO_2 GPE was ascribed to the high porosity and typical structure with good pore interconnectivity, resulting in an increase amount of the electrolyte uptake.

To evaluate the electrochemical properties of the PVDF-HFP-PEO-SiO_2 GPE, the cycling stability and rate capability were examined by CR2032 coin-type half-cells. The schematic of $LiFePO_4$/PVDF-HFP-PEO-SiO_2 GPE/Li battery is shown in Fig. 6a. The electrochemical properties of the $LiFePO_4$/GPEs/Li cells were examined at a constant current density, as shown in Fig. 6b–e. For comparison, the battery assembled with the Celgard 2325 separator that absorbed liquid electrolyte was denoted by $LiFePO_4$/Celgard 2325 separator/Li. Fig. 6b depicts the initial charge/discharge curves of the cells with various GPEs. The same charge/discharge voltage plateaus were found in the curves, while the battery with PVDF-HFP-PEO-SiO_2 GPE exhibited the highest discharge capacity of 152.5 mA h g^{-1} and initial coulombic efficiency of 94.5%. Fig. 6c displays the cycling stability of the $LiFePO_4$/GPEs/Li cells in a voltage range between 2.6 and 4.0 V at a current density of 0.1C. It was found that the discharge capacity of the cell with PVDF-HFP-PEO-SiO_2 GPE reached a high capacity of 146.3 mA h g^{-1} even after 200 cycles,

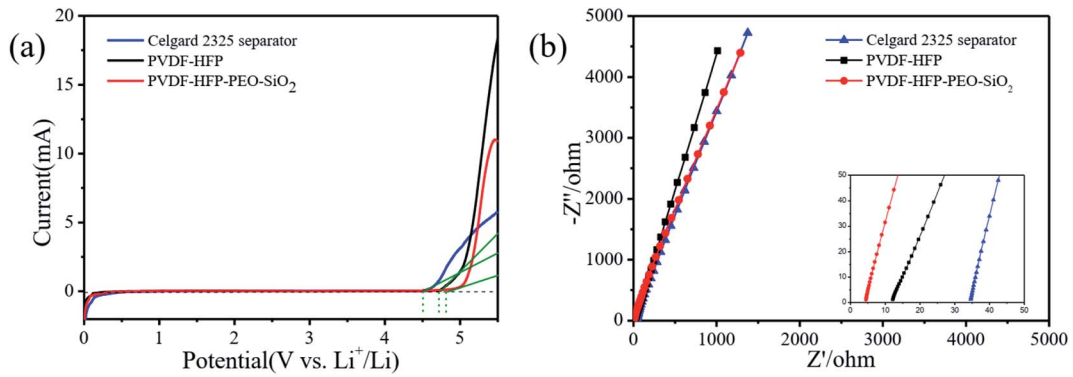

Fig. 4 (a) LSV curves and (b) impedance spectra of the Celgard 2325 separator absorbed liquid electrolyte and PVDF-HFP-based GPEs.

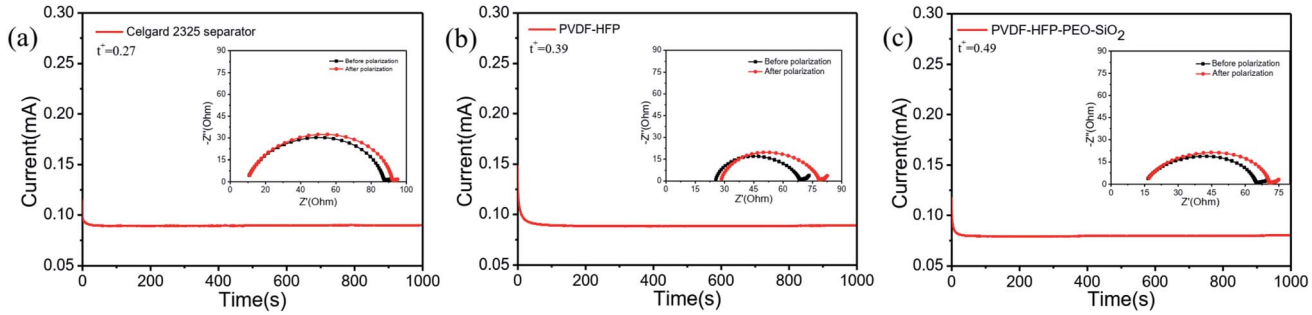

Fig. 5 Chronoamperometry curves of (a) Celgard 2325 separator, (b) PVDF-HFP, (c) PVDF-HFP-PEO-SiO_2 in the symmetrical Li/GPE/Li cells. AC impedances before and after polarization are shown in the inset.

with the capacity retention of ~100%. For comparison, the $LiFePO_4$/Celgard 2325 separator/Li cell showed a significant capacity fading after 50 cycles, and remained the discharge capacity of 85.8 mA h g^{-1} after 200 cycles, with the capacity retention of only 58%. The $LiFePO_4$/PVDF-HFP GPE/Li cell exhibited a serious capacity fading after 30 cycles, and only retained the capacity of ~50 mA h g^{-1} after 100 cycles. Fig. 6d shows the discharge capacities of cells at different rates from

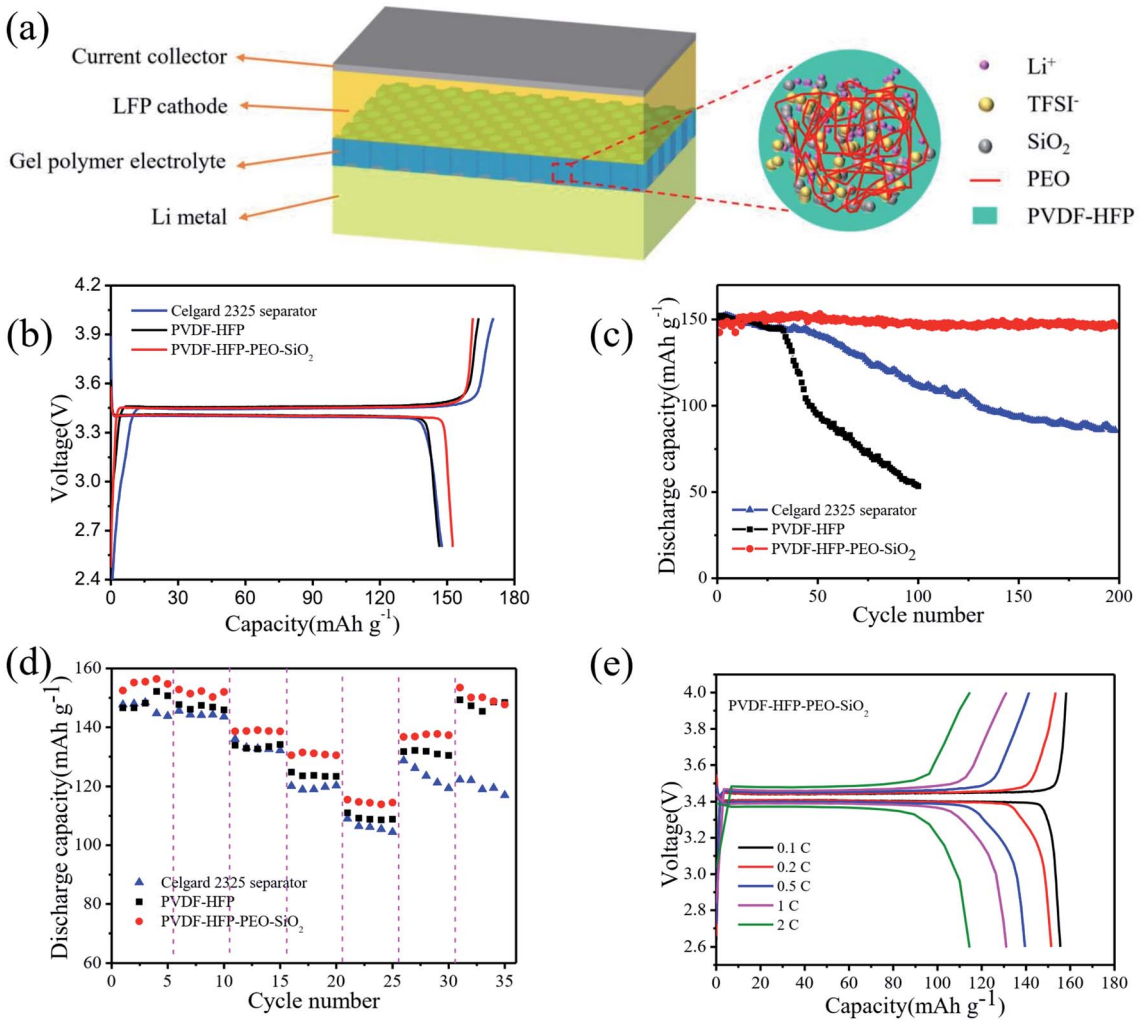

Fig. 6 (a) Schematic illustration of $LiFePO_4$/PVDF-HFP-PEO-SiO_2 GPE/Li battery and PVDF-HFP-PEO-SiO_2 membrane. (b) Charge and discharge curves of $LiFePO_4$/GPEs/Li cells during the first cycle. (c) Cycling performance of $LiFePO_4$/GPEs/Li cells for 200 cycles at 0.1C rate. (d) Rate capability of $LiFePO_4$/GPE/Li cells based on Celgard 2325 separator, PVDF-HFP, and PVDF-HFP-PEO-SiO_2 GPEs. (e) Charge and discharge curves of $LiFePO_4$/PVDF-HFP-PEO-SiO_2 GPE/Li cell at various current densities from 0.1C to 2C.

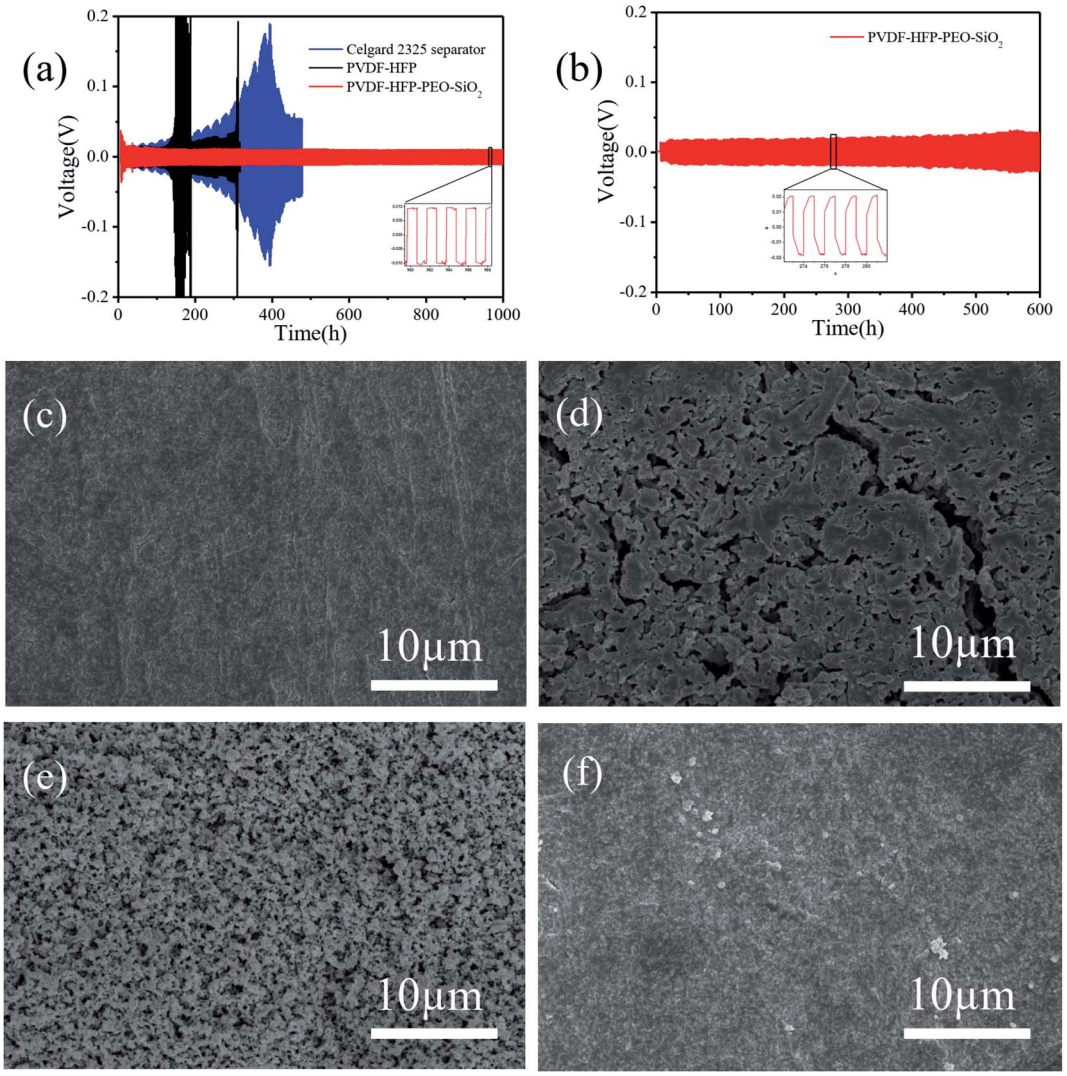

Fig. 7 (a) Voltage profiles of the lithium plating/striping cycling of symmetrical Li/Li cells with Celgard 2325 separator, PVDF-HFP and PVDF-HFP-PEO-SiO_2 GPEs at a current density of 0.1 mA cm^{-2}. (b) Voltage profiles of the lithium plating/striping cycling of PVDF-HFP-PEO-SiO_2 GPE at a current density of 0.2 mA cm^{-2}. SEM images of (c) Li metal before cycling, (d) Li metal of Li/Celgard 2325 separator/Li cell after 500 h cycles, (e) Li metal of Li/PVDF-HFP GPE/Li cell after 310 h cycles, and (f) Li metal of Li/PVDF-HFP-PEO-SiO_2 GPE/Li cell after 1000 h cycles at a current density of 0.1 mA cm^{-2}.

0.1C to 2C. It can be seen that PVDF-HFP-PEO-SiO_2 GPE showed outstanding rate performance. Its discharge capacity was 115.5 mA h g^{-1} even at a high rate of 2C, which was higher than $LiFePO_4$/Celgard 2325 separator/Li cell (109 mA h g^{-1}). When the current density was returned to 0.1C, the discharge capacity of $LiFePO_4$/PVDF-HFP-PEO-SiO_2 GPE/Li cell recovered to 147.7 mA h g^{-1}, while $LiFePO_4$/Celgard 2325 separator/Li cell exhibited a low capacity of 117 mA h g^{-1}. Fig. 6e shows the charge/discharge profiles of $LiFePO_4$/PVDF-HFP-PEO-SiO_2 GPE/Li cell at various current densities from 0.1 to 2C. The overpotential slightly increased with the increase of current density, showing a relatively low polarization. This enhanced rate capability was attributed to the high ionic conductivity and lithium-ion transference number of PVDF-HFP-PEO-SiO_2 GPE.[3,11] Therefore, the PVDF-HFP-PEO-SiO_2 GPE with the great rate capability and excellent cycling stability can be considered as a candidate for the high-performance electrolyte in LIBs.

The long-term electrochemical stability of GPEs against the Li dendrites growth was evaluated by the Li/GPEs/Li cells. Fig. 7a presents the lithium plating/striping voltage profile of the symmetric cells under a current density of 0.1 mA cm^{-2}. Obviously, the Li/PVDF-HFP-PEO-SiO_2 GPE/Li symmetric cell exhibited low polarization voltage after 1000 h of cycles, and also no short-circuit phenomenon occurred. For comparison, the overpotential of the Celgard 2325 separator saturated with the liquid electrolyte gradually increased in the first 400 h of cycles and then dropped significantly, while the overpotential of PVDF-HFP increased sharply after only 150 h of cycles, implied that a severe lithium dendrite growth happened to further cause short-circuit. Furthermore, the Li/PVDF-HFP-PEO-SiO_2 GPE/Li symmetric cell also can be stably cycled for 600 h at a high

current density of 0.2 mA cm^{-2} (Fig. 7b). SEM images of the lithium metals before and after cycling for various symmetric cells are shown in Fig. 7c–f. It can be seen that the surface of the lithium metal was smooth before cycling (Fig. 7c). After 500 h cycling, cracks and uneven lithium deposition of lithium were found for the cell assembled with the Celgard 2325 separator absorbed liquid electrolyte (Fig. 7d). Meanwhile, the lithium metal of Li/PVDF-HFP GPE/Li cell after being cycled for 300 h exhibited massive and particulate lithium crystal, as shown in Fig. 7e. In surprise, the surface of the lithium metal of Li/PVDF-HFP-PEO-SiO_2 GPE/Li cell was still relatively smooth even after 1000 h cycles, in which the growth of lithium dendrite was not observed (Fig. 7f). Based on these results, the typical structure of PVDF-HFP-PEO-SiO_2 GPE effectively inhibited the lithium dendrite growth, thereby improving the safety of the lithium metal batteries.[3]

4. Conclusions

We have developed a PVDF-HFP-PEO-SiO_2 composite membrane with porous structure by immersion precipitation method. By having the advantage of a finger-like porous structure with high porosity, this designed membrane can effectively improve liquid electrolyte uptake, resulting in the high ionic conductivity of 1.12×10^{-3} S cm^{-1} and lithium-ion transference number (t_{Li^+}) of 0.48. Hence, the outstanding cycling performance (147.7 mA h g^{-1} after 200 cycles) was demonstrated using the $LiFePO_4$ cathode based on the PVDF-HFP-PEO-SiO_2 GPE. Moreover, it can assist in inhibition of the growth of lithium dendrites, resulting in a superior compatibility with lithium metal. Taking the facile fabrication process and the eco-friendly and low-cost qualities in account, this novel developed GPE has a great potential to be utilized for high-performance and safety LIBs.

Conflicts of interest

There are no conflicts to declare.

Acknowledgements

This work was financially supported by the National Natural Science Foundation of China (21606135), the Science Technology Innovation Research Program of Ningbo (2019B10113, 2020Z024). This work was also sponsored by K. C. Wong Magna Fund in Ningbo University.

References

1 G. H. Chen, F. Zhang, Z. M. Zhou, J. R. Li and Y. B. Tang, A Flexible Dual-Ion Battery Based on PVDF-HFP-Modified Gel Polymer Electrolyte with Excellent Cycling Performance and Superior Rate Capability, *Adv. Energy Mater.*, 2018, **8**, 1801219.

2 H. S. Jeong and S. Y. Lee, Closely packed SiO2 nanoparticles/poly(vinylidene fluoride-hexafluoropropylene) layers-coated polyethylene separators for lithium-ion batteries, *J. Power Sources*, 2011, **196**, 6716–6722.

3 Y. Li, W. Zhang, Q. Q. Dou, K. W. Wong and K. M. Ng, Li7La3Zr2O12 ceramic nanofiber-incorporated composite polymer electrolytes for lithium metal batteries (vol 7, pg 4190, 2019), *J. Mater. Chem. A*, 2019, **7**, 4190.

4 S. H. Yi, T. H. Xu, L. Li, M. M. Gao, K. Du, H. L. Zhao and Y. Bai, Fast ion conductor modified double-polymer (PVDF and PEO) matrix electrolyte for solid lithium-ion batteries, *Solid State Ionics*, 2020, **355**, 115419.

5 P. Bose, D. Deb and S. Bhattacharya, Lithium-polymer battery with ionic liquid tethered nanoparticles incorporated P(VDF-HFP) nanocomposite gel polymer electrolyte, *Electrochim. Acta*, 2019, **319**, 753–765.

6 T. Famprikis, P. Canepa, J. A. Dawson, M. S. Islam and C. Masquelier, Fundamentals of inorganic solid-state electrolytes for batteries, *Nat. Mater.*, 2019, **18**, 1278–1291.

7 H. H. Xu, P. H. Chien, J. J. Shi, Y. T. Li, N. Wu, Y. Y. Liu, Y. Y. Hu and J. B. Goodenough, High-performance all-solid-state batteries enabled by salt bonding to perovskite in poly(ethylene oxide), *Proc. Natl. Acad. Sci. U. S. A.*, 2019, **116**, 18815–18821.

8 Z. Wan, D. Lei, W. Yang, C. Liu, K. Shi, X. Hao, L. Shen, W. Lv, B. Li, Q.-H. Yang, F. Kang and Y.-B. He, Low Resistance-Integrated All-Solid-State Battery Achieved by Li7La3Zr2O12 Nanowire Upgrading Polyethylene Oxide (PEO) Composite Electrolyte and PEO Cathode Binder, *Adv. Funct. Mater.*, 2019, **29**, 1805301.

9 X. Pan, T. Liu, D. J. Kautz, L. Mu, C. Tian, T. E. Long, P. Yang and F. Lin, High-performance N-methyl-N-propylpiperidinium bis (trifluoromethanesulfonyl)imide/poly(vinylidene fluoride-hexafluoropropylene) gel polymer electrolytes for lithium metal batteries, *J. Power Sources*, 2018, **403**, 127–136.

10 Q. Lu, L. N. Dong, L. Y. Chen, J. F. Fu, L. Y. Shi, M. M. Li, X. F. Zeng, H. Lei and F. Zheng, Inorganic-organic gel electrolytes with 3D cross-linking star-shaped structured networks for lithium ion batteries, *Chem. Eng. J.*, 2020, **393**, 124708.

11 J. Jie, Y. Liu, L. Cong, B. Zhang, W. Lu, X. Zhang, J. Liu, H. Xie and L. Sun, High-performance PVDF-HFP based gel polymer electrolyte with a safe solvent in Li metal polymer battery, *J. Energy Chem.*, 2020, **49**, 80–88.

12 P. Xu, H. Chen, X. Zhou and H. Xiang, Gel polymer electrolyte based on PVDF-HFP matrix composited with rGO-PEG-NH2 for high-performance lithium ion battery, *J. Membr. Sci.*, 2021, **617**, 118660.

13 Z. Y. Kou, C. J. Liu, C. Miao, P. Mei, X. M. Yan and W. Xiao, High-performance gel polymer electrolytes using P(VDF-HFP) doped with appropriate porous carbon powders as the matrix for lithium-ion batteries, *Ionics*, 2020, **26**, 1729–1737.

14 S. Ferrari, E. Quartarone, P. Mustarelli, A. Magistris, M. Fagnoni, S. Protti, C. Gerbaldi and A. Spinella, Lithium ion conducting PVdF-HFP composite gel electrolytes based on N-methoxyethyl-N-methylpyrrolidinium

bis(trifluoromethanesulfonyl)-imide ionic liquid, *J. Power Sources*, 2010, **195**, 559–566.

15 W. H. Pu, X. M. He, L. Wang, C. Y. Jiang and C. R. Wan, Preparation of PVDF-HFP microporous membrane for Li-ion batteries by phase inversion, *J. Membr. Sci.*, 2006, **272**, 11–14.

16 A. M. Stephan, Review on gel polymer electrolytes for lithium batteries, *Eur. Polym. J.*, 2006, **42**, 21–42.

17 J. L. Li, L. Zhu, J. N. Xu, M. X. Jing, S. S. Yao, X. Q. Shen, S. J. Li and F. Y. Tu, Boosting the performance of poly(ethylene oxide)-based solid polymer electrolytes by blending with poly(vinylidene fluoride-co-hexafluoropropylene) for solid-state lithium-ion batteries, *Int. J. Energy Res.*, 2020, **44**, 7831–7840.

18 Z. J. Wang, K. Yang, Y. L. Song, H. Lin, K. Li, Y. H. Cui, L. Y. Yang and F. Pan, Polymer matrix mediated solvation of LiNO3 in carbonate electrolytes for quasi-solid high-voltage lithium metal batteries, *Nano Res.*, 2020, **13**, 2431–2437.

19 J. Li, R. Hu, H. Zhou, S. Tao and Y. Wang, Nano-SiO2@PMMA-doped composite polymer PVDF-HFP/PMMA/PEO electrolyte for lithium metal batteries, *J. Mater. Sci.: Mater. Electron.*, 2020, **31**, 2708–2719.

20 T. Yang, C. Shu, R. Zheng, M. Li, Z. Hou, P. Hei, Q. Zhang, D. Mei and J. Long, Dendrite-Free Solid-State Li-O-2 Batteries Enabled by Organic-Inorganic Interaction Reinforced Gel Polymer Electrolyte, *ACS Sustainable Chem. Eng.*, 2019, **7**, 17362–17371.

21 C. M. S. Prasanna and S. A. Suthanthiraraj, Improved zinc ion transportation in gel polymer electrolyte upon the addition of nano-sized SnO2, *Polym. Polym. Compos.*, 2020, **28**, 54–65.

22 X. L. Wang, X. J. Hao, Y. Xia, Y. F. Liang, X. H. Xia and J. P. Tu, A polyacrylonitrile (PAN)-based double-layer multifunctional gel polymer electrolyte for lithium-sulfur batteries, *J. Membr. Sci.*, 2019, **582**, 37–47.

23 X. L. Fu, C. Q. Shang, M. Y. Yang, E. M. Akinoglu, X. Wang and G. F. Zhou, An ion-conductive separator for high safety Li metal batteries, *J. Power Sources*, 2020, **475**, 228687.

24 B. Li, Y. Huang, P. Cheng, B. Liu, Z. Yin, Y. Lin, X. Li, M. Wang, H. Cao and Y. Wu, Upgrading comprehensive performances of gel polymer electrolyte based on polyacrylonitrile via copolymerizing acrylonitrile with N-vinylpryrrolidone, *Electrochim. Acta*, 2019, **320**, 134572.

25 C. Fasciani, S. Panero, J. Hassoun and B. Scrosati, Novel configuration of poly(vinylidenedifluoride)-based gel polymer electrolyte for application in lithium-ion batteries, *J. Power Sources*, 2015, **294**, 180–186.

26 D. Xu, J. M. Su, J. Jin, C. Sun, Y. D. Ruan, C. H. Chen and Z. Y. Wen, In Situ Generated Fireproof Gel Polymer Electrolyte with Li6.4Ga0.2La3Zr2O12 As Initiator and Ion-Conductive Filler, *Adv. Energy Mater.*, 2019, **9**, 1900611.

27 X. L. Wang, X. J. Hao, D. Cai, S. Z. Zhang, X. H. Xia and J. P. Tu, An ultraviolet polymerized 3D gel polymer electrolyte based on multi-walled carbon nanotubes doped double polymer matrices for lithium-sulfur batteries, *Chem. Eng. J.*, 2020, **382**, 122714.

28 F. Zhang, X. L. Ma, C. B. Cao, J. L. Li and Y. Q. Zhu, Poly(vinylidene fluoride)/SiO2 composite membranes prepared by electrospinning and their excellent properties for nonwoven separators for lithium-ion batteries, *J. Power Sources*, 2014, **251**, 423–431.

29 Y. Liu, J. Y. Lee and L. Hong, In situ preparation of poly(ethylene oxide)-SiO2 composite polymer electrolytes, *J. Power Sources*, 2004, **129**, 303–311.

30 Y. H. Jiang, F. Li, Y. F. Mei, Y. H. Ding, H. J. Pang and P. Zhang, Gel polymer electrolyte based on hydrophilic-lipophilic TiO2-modified thermoplastic polyurethane for high-performance Li-ion batteries, *J. Mater. Sci.*, 2021, **56**, 2474–2485.

31 R. Tian, X. Q. Feng, H. N. Duan, P. Zhang, H. Li, H. Z. Liu and L. Gao, Low-Weight 3D Al2O3 Network as an Artificial Layer to Stabilize Lithium Deposition, *Chemsuschem*, 2018, **11**, 3243–3252.

32 L. Liu, Y. Wang, C. Y. Gao, C. Yang, K. Wang, H. B. Li and H. T. Gu, Ultrathin ZrO2-coated separators based on surface sol-gel process for advanced lithium ion batteries, *J. Membr. Sci.*, 2019, **592**, 117368.

33 E. Fontananova, J. C. Jansen, A. Cristiano, E. Curcio and E. Drioli, Effect of additives in the casting solution on the formation of PVDF membranes, *Desalination*, 2006, **192**, 190–197.

34 S. Rajabi, F. Khodadadi, T. Mohammadi, M. Tavakolmoghadam and F. Rekabdar, Morphology control in PVDF membranes using PEG/PVP additives and mixed solvents, *Membrane and Water Treatment*, 2020, **11**, 237–245.

35 D.-y. Zuo, Y.-y. Xu, W.-l. Xu and H.-t. Zou, The influence of PEG molecular weight on morphologies and properties of PVDF asymmetric membranes, *Chin. J. Polym. Sci.*, 2008, **26**, 405–414.

36 Z. Y. Hu, J. J. Chen, Y. Guo, J. J. Zhu, X. X. Qu, W. W. Niu and X. K. Liu, Fire-resistant, high-performance gel polymer electrolytes derived from poly (ionic liquid)/P(VDF-HFP) composite membranes for lithium ion batteries, *J. Membr. Sci.*, 2020, **599**, 117827.

37 S. Caimi, A. Klaue, H. Wu and M. Morbidelli, Effect of SiO2 Nanoparticles on the Performance of PVdF-HFP/Ionic Liquid Separator for Lithium-Ion Batteries, *Nanomaterials*, 2018, **8**, 926.